J. Earth Planet. Sci. Nagoya Univ., Vol. 44, 61 to 69, 1997

CHIME ages of zircons in granitic gneiss and granite from Samilpo, southeastern Democratic People's Republic of Korea

Takenori KATO*, Kazuhiro SUZUKI*, Taisei MORISHITA*
and Chinatsu YONEZAWA**

** Department of Earth and Planetary Sciences, Graduate School ofScience, Nagoya University, Nagoya, 464-01, Japan*
*** Remote Sensing Technology Center of Japan, 1-9-9, Roppongi, Minato-ku, Tokyo 106, Japan*
(Received September 19, 1997 / Accepted October 24, 1997)

ABSTRACT

The CHIME (chemical Th-U-total Pb isochron method) dating was carried out for zircons from pyrope-rich (Prp_{28} – Prp_{32}) garnet-bearing granitic gneiss and topaz-bearing biotite granite from the Samilpo region in the southeastern part of Democratic People's Republic of Korea. Zircons from the garnet--bearing granitic gneiss show a distinct core-rim structure; the cores yield an early Proterozoic age of 2133 ± 56 Ma, and the rims yield a poorly refined age of ca. 1500 Ma. The core and rim ages agree well with those for protolith formation and high-grade metamorphism, respectively, of the basement gneiss complex in the Gyeonggi Massif. Zircons from the topaz-bearing granite show a middle Jurassic age of 172 ± 4 Ma, suggesting the granite to be assigned to the Jurassic Daebo Granite.

INTRODUCTION

The Gyeonggi Massif occupies the central part of the Korean Peninsula, and together with the Nangrim and Yeongnam Massifs, it is one of the major tectonic units where middle Proterozoic metamorphic rocks widely occur (Na and Lee, 1973; Lee et al., 1974; Na, 1977; Cho et al., 1995; Chwae et al., 1996; Turek and Kim, 1996). In the northern part of the Gyeonggi Massif, there lies the Imjingang Fold Belt as shown in Fig. 1 (Ri and Ri, 1990). This belt involves the Sangwon Supergroup, the Joseon Supergroup and the Yeoncheon Group (or the Rimjin System), and is characterized by an EW structural trend. Recent geochronological studies revealed that rocks in the Imjingang Fold Belt have undergone, at least partly, the greenschist to amphibolite facies metamorphism at ca. 250 Ma (Cho et al., 1995; Ree et al., 1996; Cho et al., 1996). Thus, many authors consider that the Imjingang Fold Belt is an eastward continuation of the Dabie _ Su-Lu collisional belt in China and extends in EW direction to the east coast of the Korean Peninsula (Ri and Ri, 1990; Cluzel et al., 1991; Cluzel, 1992; Liu, 1993; Yin and Nie, 1993; Ernst et al., 1994; Cho et al., 1995; Ree et al., 1996). If this is the case, the Gyeonggi and Nangrim Massifs

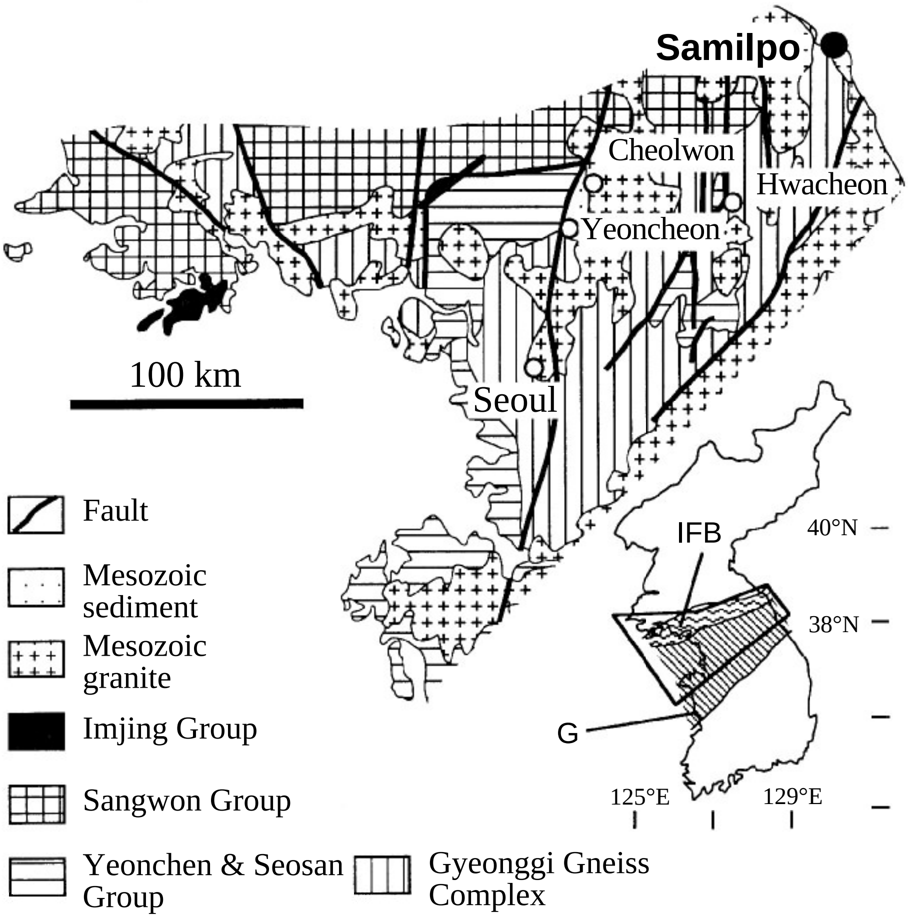

Fig. 1. Geological map of the Gyeonggi Massif. G: the Gyeonggi Massif, and IFB: the Imjing Fold Belt.

are totally different tectonic units before their collision at ca. 250 Ma. In this connection, more geochronological data are indispensable on the Gyeonggi and Nangrim massifs. However, little chronological data are available on basement rocks in Democratic People's Republic of Korea (D. P. R. K.).

To shed more light on the tectonic setting of the Korean peninsula, we determined the CHIME ages of zircons from granitic gneiss and granite from the Samilpo region, southeastern D. P. R. K. The Samilpo region is located within the postulated extension of the Imjingang Fold Belt (Fig. 1). This paper reports the preliminary age results, and will discuss the problem whether the Imjingang Fold Belt runs through the Korean Peninsula to the east coast or not.

SAMPLE DESCRIPTION

Samples collected from the coast of Samilpo are garnet-bearing granitic gneiss and topaz-bearing biotite granite. The detailed occurrences of these samples are unclear.

The sample of garnet-bearing granitic gneiss is leucocratic and has a tonalitic modal composition; it consists mainly of quartz (51%) and plagioclase (44%) with trace amounts of garnet, biotite, muscovite and zircon. Quartz forms anhedral grains, and some grains recrystallize with remnants of vaguely outlined original form. Plagioclase, about 2 mm in size, ranges in composition from An_{28} to An_{34}, and is replaced by fine-grained muscovite flakes along cleavage and twining plane. Garnet occurs as euhedral grains up to 5 mm in size, and is pyrope - almandine solid solution (Alm_{61}–Alm_{66} and Prp_{28}–Prp_{33}). Most garnet grains are replaced by biotite and muscovite along grain margins and fractures. Biotite underwent extensive chloritization. Zircon occurs in garnet, quartz and plagioclase. Individual zircon grains are subrounded, and translucent to transparent.

Granite is leucocratic and coarse-grained. It consists mainly of quartz (42%), K-feldspar (37%), plagioclase (18%) and biotite (2%) with accessory topaz, zircon and ilmenite. Secondary muscovite replaces some biotite flakes and plagioclase cores. Quartz forms anhedral grains of 0.5 - 4 mm in size. K-feldspar, 0.5 - 7 mm in size, is microcline perthite with albite lamella about 35% by volume. Some K-feldspar grains include plagioclase and quartz grains. Plagioclase is euhedral, and shows little compositional zoning. Topaz occurs as inclusion in plagioclase and as tiny discrete grain in grain boundaries between major constituent phases. Zircon occurs mainly as inclusion in biotite and quartz. Most zircon grains show concentric growth zoning with metamict cores.

CHIME AGE DETERMINATION

Zircon grains in conventional polished thin sections were analyzed on JEOL JCXA-733 electron-probe microanalyzer. Accelerating voltage, probe current and probe diameter were kept at 15 kV, 0.2 µA and 5 µm, respectively. The details of the analytical procedure and the CHIME age calculation were described in Suzuki and Adachi (1991a, 1991b, 1994) and Suzuki et al. (1991, 1994). The ThO_2, UO_2 and PbO analyses together with UO_2^* values (measured UO_2 plus UO_2 equivalent of measured ThO_2) and apparent ages of zircons from the garnet-bearing granitic gneiss and topaz-bearing biotite granite are listed in Tables 1 and 2, respectively.

A total of 76 spots of 6 zircon grains (grain ID = Z01 – Z06) were analyzed for the garnet-bearing granitic gneiss. Data points for central portions of grains 1 to 6 (55 analyses) are arrayed linearly on the UO_2^* – PbO diagram (Fig. 2), and yield an isochron of 2133 56 Ma (MSWD = 0.22) with an intercept value of 0.0006 ± 0.0006. Data points for marginal portions of these grains are

Table 1. Electron microprobe analysis of ThO_2, UO_2 and PbO of zircon grains from garnet-bearing granitic gneiss.

Grain ID	Status	ThO_2 wt. %	UO_2 wt. %	PbO wt. %	Age† Ma	UO_2^* wt.%
Z01		0.011	0.035	0.0136	2116	0.0379
Z01		0.019	0.023	0.0102	2166	0.0276
Z01		0.028	0.020	0.0107	2263	0.0273
Z01		0.004	0.108	0.0349	1938	0.1090
Z01		0.015	0.055	0.0208	2106	0.0583
Z01		0.004	0.072	0.0225	1889	0.0725
Z01		0.013	0.039	0.0151	2122	0.0419
Z01		0.004	0.060	0.0210	2036	0.0615
Z01		0.012	0.064	0.0218	1950	0.0675
Z01		0.017	0.024	0.0095	1980	0.0288
Z01		0.013	0.028	0.0113	2155	0.0307
Z01		0.007	0.051	0.0170	1960	0.0523
Z01		0.007	0.028	0.0094	1894	0.0302
Z01		0.015	0.020	0.0074	1860	0.0243
Z01		0.013	0.075	0.0255	1957	0.0786
Z01	m	0.014	0.091	0.0244	1621	0.0950
Z01		0.013	0.051	0.0195	2124	0.0541
Z01	m	0.022	0.092	0.0219	1447	0.0977
Z01	m	0.029	0.091	0.0218	1429	0.0987
Z01	m	0.009	0.037	0.0106	1677	0.0396
Z01	m	0.015	0.041	0.0110	1550	0.0452
Z01	m	0.017	0.049	0.0112	1358	0.0538
Z02		0.076	0.056	0.0281	2168	0.0758
Z02		0.008	0.047	0.0192	2256	0.0491
Z02		0.021	0.032	0.0113	1839	0.0377
Z02		0.041	0.043	0.0209	2258	0.0534
Z02		0.020	0.026	0.0095	1867	0.0311
Z02		0.012	0.029	0.0110	2057	0.0318
Z02	m	0.009	0.129	0.0266	1325	0.1315
Z02	m	0.014	0.020	0.0044	1247	0.0233
Z03		0.004	0.015	0.0049	1881	0.0159
Z03		0.009	0.020	0.0074	973	0.0226
Z03	m	0.009	0.052	0.0140	1638	0.0538
Z03	m	0.015	0.070	0.0141	1259	0.0740
Z03		0.013	0.040	0.0159	2167	0.0429
Z03		0.008	0.014	0.0047	1855	0.0155
Z03	m	0.004	0.056	0.0094	1109	0.0569
Z03	m	0.005	0.049	0.0067	918	0.0501
Z03	m	0.029	0.111	0.0238	1312	0.1191
Z03	m	0.005	0.069	0.0155	1426	0.0703
Z03		0.004	0.062	0.0212	2013	0.0630
Z03	m	0.011	0.053	0.0150	1676	0.0561
Z03	m	0.005	0.062	0.0112	1175	0.0635
Z03	m	0.004	0.056	0.0127	1441	0.0569
Z04		0.012	0.028	0.0122	2276	0.0308
Z04		0.004	0.057	0.0188	1961	0.0578
Z04		0.016	0.041	0.0170	2220	0.0445
Z04		0.014	0.043	0.0183	2278	0.0462
Z05		0.005	0.093	0.0306	1952	0.0946
Z05		0.011	0.097	0.0322	1954	0.0995
Z05		0.023	0.070	0.0292	2224	0.0761
Z05		0.146	0.272	0.1119	2127	0.3097
Z05		0.018	0.053	0.0225	2258	0.0575
Z05		0.013	0.062	0.0236	2123	0.0655
Z05		0.024	0.052	0.0211	2130	0.0583
Z05		0.192	0.332	0.1441	2203	0.3806
Z05		0.007	0.014	0.0064	2323	0.0157
Z05		0.010	0.071	0.0254	2054	0.0736
Z05	m	0.007	0.084	0.0146	1140	0.0857
Z05	m	0.009	0.023	0.0047	1239	0.0251
Z05	m	0.016	0.047	0.0077	1006	0.0520
Z06	m	0.009	0.065	0.0121	1197	0.0672
Z06		0.008	0.070	0.0245	2027	0.0722
Z06		0.020	0.066	0.0282	2277	0.0713
Z06		0.030	0.081	0.0334	2195	0.0887
Z06		0.021	0.022	0.0107	2248	0.0275
Z06		0.028	0.062	0.0222	1936	0.0694
Z06		0.013	0.027	0.0106	2088	0.0301
Z06		0.018	0.023	0.0084	1849	0.0278
Z06		0.015	0.034	0.0140	2149	0.0382
Z06		0.018	0.026	0.0101	1966	0.0309
Z06		0.013	0.022	0.0086	2031	0.0253
Z06		0.012	0.035	0.0131	2050	0.0381
Z06		0.018	0.035	0.0152	2231	0.0395
Z06		0.021	0.026	0.0116	2168	0.0313
Z06		0.022	0.037	0.0149	2056	0.0431
Z07	rm	0.005	0.069	0.0098	948	0.0708
Z07	rm	0.012	0.065	0.0116	1133	0.0686
Z07	rm	0.009	0.061	0.0083	901	0.0634
Z07	rm	0.006	0.048	0.0081	1102	0.0494
Z07	r	0.028	0.028	0.0092	1644	0.0352
Z07	r	0.008	0.023	0.0059	1516	0.0249
Z07	r	0.009	0.027	0.0072	1555	0.0295
Z07	r	0.017	0.040	0.0103	1492	0.0443
Z07	r	0.010	0.030	0.0080	1572	0.0323
Z07	r	0.006	0.018	0.0041	1368	0.0195
Z07	r	0.010	0.033	0.0096	1681	0.0358
Z07	r	0.008	0.026	0.0081	1787	0.0280
Z07	r	0.006	0.059	0.0157	1631	0.0607
Z07	r	0.037	0.070	0.0166	1350	0.0803
Z07	r	0.005	0.073	0.0186	1578	0.0748
Z07	m	0.046	0.070	0.0210	1608	0.0826
Z07	m	0.013	0.116	0.0283	1515	0.1196
Z07	m	0.058	0.210	0.0753	2004	0.2252
Z07		0.050	0.077	0.0318	2098	0.0896
Z07		0.058	0.071	0.0287	1997	0.0862
Z07		0.038	0.060	0.0271	2249	0.0696
Z07		0.005	0.060	0.0132	1398	0.0613
Z07		0.013	0.123	0.0435	2052	0.1262
Z07		0.039	0.053	0.0218	2045	0.0635
Z07	m	0.021	0.164	0.0520	1874	0.1694
Z07		0.006	0.057	0.0121	1355	0.0583
Z07		0.006	0.076	0.0159	1343	0.0774
Z07		0.007	0.076	0.0189	1544	0.0781
Z07		0.012	0.072	0.0166	1430	0.0751

UO_2^*: sum of ThO_2 and UO_2 equivalent of UO_2
Age†: apparent age
Staus shows: r = rim of grain and m = metamict, respectively.

plotted below the 2133 Ma isochron, and yield poorly defined isochron of 1431 ± 184 Ma (MSWD = 0.83).

To know the age zoning within zircon grains, detailed analyses were carried out on another grain (grain ID = Z07). This grain shows a distinct core-rim structure; the core is characterized by concentric zones of variable Y and Hf concentrations, and the rim by a homogeneous Y and Hf distribution. The Y- and Hf-distribution patterns in the core, presumably resulted from growth zoning at the igneous stage, are crosscut by the homogeneous rim. As shown in Fig. 3, seven data points for the core define an isochron of 1976 ± 222 Ma

Table 2. Electron microprobe analyses of ThO_2, UO_2 and PbO of zircon grains from topaz-bearing biotite granite.

Grain ID	Status	ThO_2 wt. %	UO_2 wt. %	PbO wt. %	Age† Ma	UO_2^* wt. %
Z01	m	2.073	1.083	0.0249	107	1.7286
Z01	m	1.599	2.122	0.0323	92	2.6208
Z01	m	1.833	2.711	0.0457	104	3.2826
Z01	m	0.730	1.217	0.0189	97	1.4450
Z01	m	1.244	1.321	0.0360	156	1.7074
Z01		0.250	0.550	0.0148	175	0.6276
Z01		2.001	0.584	0.0285	175	1.2049
Z01	m	1.140	2.094	0.0325	99	2.4495
Z01	m	4.042	1.457	0.0434	119	2.7154
Z01		1.053	0.778	0.0249	167	1.1045
Z01	m	0.846	1.910	0.0314	107	2.1734
Z01	m	1.741	2.679	0.0434	100	3.2217
Z01	m	2.176	3.007	0.0636	128	3.6839
Z01		1.817	2.700	0.0772	175	3.2637
Z01	m	2.166	1.728	0.0329	102	2.4031
Z01		0.947	1.774	0.0464	166	2.0673
Z01	m	1.002	1.645	0.0350	133	1.9571
Z01	m	1.668	1.318	0.0308	125	1.8374
Z01		2.928	0.899	0.0426	175	1.8066
Z01		0.369	0.452	0.0128	167	0.5664
Z01	m	0.826	1.918	0.0280	96	2.1761
Z01	m	0.945	2.038	0.0469	149	2.3316
Z01	m	2.197	1.463	0.0185	64	2.1501
Z01	m	2.005	1.233	0.0206	82	1.8590
Z01		0.540	0.697	0.0191	164	0.8643
Z01		1.246	1.116	0.0343	169	1.5025
Z01		0.868	1.044	0.0295	166	1.3138
Z01	m	0.559	0.769	0.0153	121	0.9433
Z01		0.747	0.628	0.0192	165	0.8598
Z01		0.450	0.573	0.0177	184	0.7129
Z02	m	0.438	1.215	0.0163	90	1.3521
Z02		0.439	0.520	0.0156	176	0.6565
Z02	m	0.604	0.939	0.0165	109	1.1278
Z02	m	4.055	1.635	0.0340	87	2.9003
Z02		3.362	1.500	0.0603	176	2.5424
Z02	m	0.358	0.919	0.0100	72	1.0309
Z02	m	0.132	0.538	0.0094	121	0.5790
Z02		0.771	0.589	0.0188	168	0.8287
Z02	m	0.539	0.866	0.0203	146	1.0336
Z02	m	1.713	1.152	0.0228	101	1.6864
Z02	m	1.801	1.335	0.0297	116	1.8959
Z02	m	2.248	2.127	0.0386	102	2.8275
Z02		0.926	1.387	0.0401	177	1.6743
Z02	m	1.238	1.108	0.0291	145	1.4928
Z02	m	3.463	1.479	0.0538	156	2.5542
Z02		0.249	0.745	0.0198	178	0.8223
Z02	m	0.497	0.933	0.0161	110	1.0874
Z02		0.284	0.584	0.0162	178	0.6718
Z02		0.338	0.509	0.0149	180	0.6136
Z02		0.634	1.162	0.0324	177	1.3582
Z02		0.690	1.180	0.0315	167	1.3944
Z02		0.220	0.484	0.0131	175	0.5526
Z02	m	0.193	0.743	0.0100	93	0.8037
Z02		0.097	0.276	0.0069	167	0.3064
Z02		0.125	0.269	0.0073	175	0.3081
Z03		0.286	0.178	0.0058	161	0.2662
Z03		0.094	0.269	0.0072	175	0.2985
Z03		0.083	0.250	0.0069	185	0.2757
Z03	m	0.495	0.668	0.0172	155	0.8214
Z03		0.504	0.798	0.0215	167	0.9545
Z03	m	0.125	1.793	0.0143	58	1.8320
Z03		0.113	0.510	0.0135	183	0.5446
Z03		0.183	0.297	0.0072	151	0.3541
Z03		0.097	0.267	0.0077	192	0.2966
Z03		0.134	0.263	0.0070	170	0.3049

UO_2^*: sum of ThO_2 and UO_2 equivalent of UO_2
Age†: apparent age
Staus shows: m = metamict.

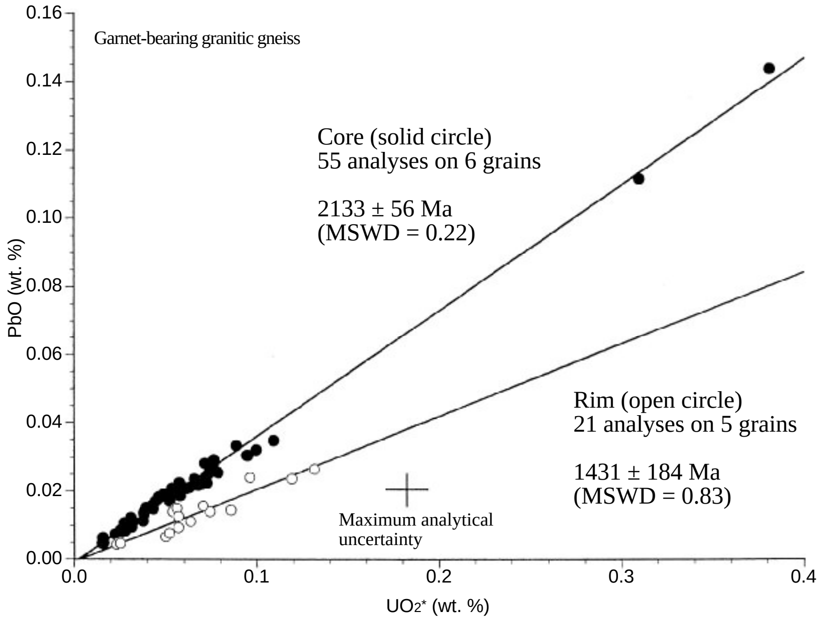

Fig. 2. UO_2^* – PbO plot of six zircon grains (grain ID = Z01 – Z06) from the pyrope-rich garnet-bearing granitic gneiss. Solid and open circles represent core and rim parts, respectively.

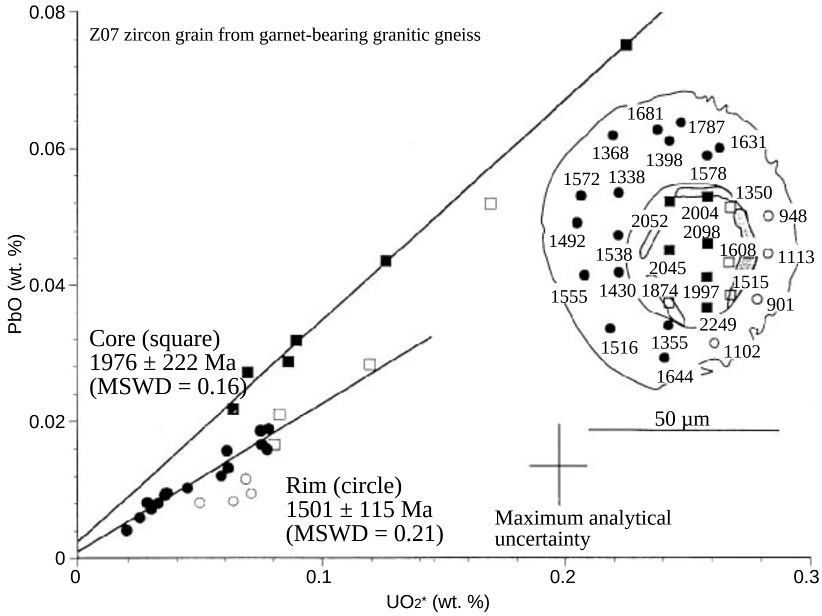

Fig. 3. UO_2* – PbO plot of a zircon grain (grain ID = Z07) from the pyrope-rich garnet-bearing granitic gneiss. Squares and circles represent core and rim parts, respectively. Filled and open marks represent transparent and metamict parts, respectively

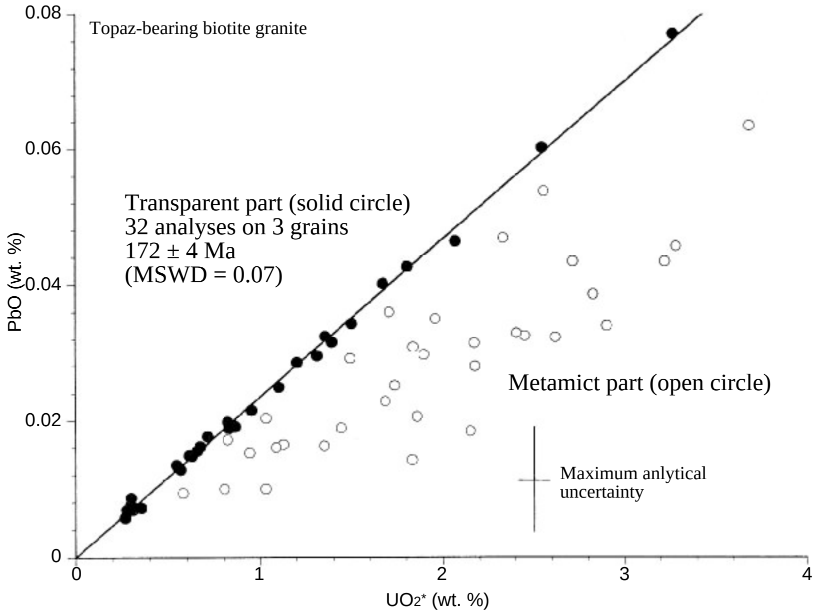

Fig. 4. UO_2* – PbO plot of zircon grains from the granite. Solid and open circles represent transparent and metamic parts, respectively.

(MSWD = 0.16), and those for the rim define an isochron of 1501 115 Ma (MSWD = 0.21). These ages are correlative to the core and rim ages in Fig. 2 within the limit of analytical error. The core age of 2133 ± 56 Ma is interpreted as the time of the protolith formation and the rim age of ca. 1500 Ma as the time of the high-grade metamorphism.

Figure 4 shows the UO_2^* – PbO plots of 65 analyses on 3 zircon grains from the topaz-bearing biotite granite. Data points on transparent portions (solid circle, 32 analyses) are regressed with a single isochron of 172 ± 4 Ma (MSWD = 0.07) with an intercept value of 0.0001 ± 0.0004. This middle Jurassic age represents the time of the granite emplacement.

DISCUSSION AND CONCLUSION

The Yeoncheon Group in the Imjingang Fold Belt underwent the greenschist to amphibolite facies metamorphism of the kyanite-sillimanite type (Na, 1979). The protolith age was determined as 824 ± 143 Ma (MSWD = 9.9) for amphibolite by the Sm-Nd whole-rock isochron method (Ree et al., 1996). Ree et al. (1996) also reported mineral isochron ages of 249 ± 3 Ma (Sm-Nd) and 221 ± 31 Ma (Rb-Sr). Cho et al. (1996) obtained a CHIME monazite age of 255 ± 8 Ma from kyanite-staurolite-garnet schist from the upper part of the Yeoncheon Group. These mineral ages agree well with one another within analytical error, and suggest that regional metamorphism in the Imjingang Fold Belt occurred during Permian – Triassic time.

The garnet-bearing granitic gneiss from the Samilpo region, as stated above, formed at 2133 Ma and underwent a high-grade metamorphism at ca. 1500 Ma. Outermost portions of individual zircon grains yield apparent ages younger than 1500 Ma, but none is younger than ca. 900 Ma (Figs. 2 and 3). It, therefore, is hard to consider that metamorphic rocks in the Samilpo region underwent the Permian-Triassic metamorphism. The core age of 2133 Ma and rim age of ca. 1500 Ma are correlative to the isotopic ages for gneisses in the Gyeonggi Gneiss Complex so far reported (Gaudette and Hurley, 1973; Hurley et al., 1973; Lan et al., 1995; Turek and Kim, 1996); the metamorphic rocks in the Samilpo region are regarded as the basement gneiss complex in the Gyeonggi Massif.

A question, here, arises regarding the eastern end of the Imjingang Fold Belt. A clear Permian – Triassic metamorphism of post-middle Proterozoic sediment can be traced eastward up to the Hwacheon area. Although paragneisses in this area have been regarded to be the Archean – early Proterozoic, the sillimanite-garnet gneiss gives a CHIME monazite age of 245 ± 3 Ma, and a monazite grain contains ca. 1700 Ma core of detrital origin (Cho et al., 1996). Since Na (1979) reported kyanite in addition to sillimanite, the metamorphic rocks in the Hwacheon area are regarded as the eastward continuation of the Yeoncheon Group. Judging from these geochronological data, we consider that the Imjingang Fold Belt does not extend to the east coast of the Korean Peninsula.

ACKNOWLEDGMENTS

We thank Drs. U. C. Chwae and D. L. Cho of KIGAM for their discussion of the geologic setting of the Korean Peninsula, and Dr. K. Shibata of Nagoya Bunri College and an anonymous reviewer for their thoughtful comments. We also thank Mr. S. Yogo of Nagoya University for his excellent technical assistance.

REFERENCES

Cho, D. L., Kwon, S. T., Ree, J. H. and Nakamura, E. (1995) High pressure amphibolite of the Imjingang belt in the Yeoncheon-Cheongok are. *J. Petrol. Soc. Korea*, **4**, 1 – 19.

Cho, D. L., Suzuki, K., Adachi, M. and Chwae, U.-C. (1996) A preliminary CHIME age deter mination of monazites from metamorphic and granitic rocks in the Gyeonggi Massif, Korea. *J. Earth Planet. Sci., Nagoya Univ.*, **43**, 49 – 65.

Chwae, U.-C., Choi, S. J., Park, K. H. and Kim, K. B. (1996) Explanatory text of the geological map of Cheolwon-Majeonri sheets (scale 1:50,000). Korea Inst. Geol. Mining and Materials, 1 – 31.

Cluzel, D. (1992) Ordovician bimodal magmatism in the Ogcheon belt (South Korea): Intracontinental rift related volcanic activity. *J. Southeast Asian Earth Sci.*, **7**, 195 – 209.

Cluzel, D., Lee, B. J. and Cadet, J. P. (1991) Indosinian dextral ductile fault system and synkinematic plutonism in the southwest of the Ogcheon blet (South Korea). *Tectonophysics*, **194**, 131 – 152.

Ernst, W. G., Liou, J. G. and Harker, B. R. (1994) Petrotectonic significance of high- and ultrahigh-pressure metamorphic belts: Inferences for subduction zone history. *Int. Geol. Rev.*, **36**, 213 – 237.

Gaudette, F. E. and Hurley, P. M. (1973) U-Pb zircon age of Precambrian basement gneiss of South Korea. *Geol. Soc. Am. Bull.*, **84**, 2305 – 2306.

Hurley, P. M., Fairbairn, H. W., Pinson, Jr., W. H. and Lee, J. H. (1973) Middle Precambrian and older apparent age values in basement gneiss of South Korea, and relations with Southwest Japan. *Geol. Soc. Am. Bull.*, **84**, 2229 – 2303.

Lan, C. N., Lee, T., Zhow, X. H. and Kwan, S. T. (1995) Nd isotopic study of Precambrian basement of South Korea: evidence for early Archean crust? *Geology*, **23**, 249 – 252.

Lee, D. S., Lee, H. Y., Nam, K. S. and Yang, S. Y. (1974) Explanatory text of the geological map of Chucheon sheet (scale 1:50,000). Geol. and Mineral Inst. Korea, 1 – 9.

Liu, X. (1993) High-P metamorphic belt in central China and its possible eastward extension to Korea. *J. Petrol. Soc. Korea*, **2**, 9 – 18.

Na, K. C. (1977) The geology and granitization of northeastern Gyeonggi Massif. *Res. Rev. Chungbuk Univ.*, **15**, 57 – 66.

Na, K. C. (1979) Regional metamorphism in Gyeonggi Massif with comparative studies between Yenchen and Okcheon metamorphic belts (II). *J. Geol. Soc. Korea*, **15**, 67 – 88.

Na, K. C. and Lee, D. J. (1973) Preliminary age study of the Gyeonggi metamorphic belt by the Rb-Sr whole rock method. *J. Geol. Soc. Korea*, **19**, 168 – 174.

Ree, J.-H., Cho, M., Kwon, S.-T. and Nakamura, E. (1996)Possible eastward extension of Chinese collision blet in South Korea: The Imjingang blet. *Geology*, **23**, 1071 – 1074.

Ri, J. N. and Ri, J. C. (1990) Geological constitution of Korea. Industrial Publishing House, **6**, 216pp.

Suzuki, K. and Adachi, M. (1991a) Precambrian provenance and Silurian metamorphism of the Tsubonosawa paragneiss in the South Kitakami terrane, Northeast Japan, revealed by the chemical Th-U-total Pb isochron ages of monazite, zircon and xenotime. *Geochem. J*, **25**, 357 – 376.

Suzuki, K. and Adachi, M. (1991b) The chemical Th-U-total Pb isochron ages of zircon and monazite from the Gray Granite of the Hida terrane, Japan. *J. Earth Sci., Nagoya Univ.*, **38**, 11 – 37.

Suzuki, K. and Adachi, M. (1994) Middle Precambrian detrital monazite and zircon from the Hida gneiss on Oki-Dogo Island, Japan: their origin and implications for the correlation of basement gneiss of Southwest Japan and Korea. *Tectonophysics*, **235**, 277 – 292.

Suzuki, K., Adachi, M. and Kajizuka, I. (1994) Electron microprobe observations of Pb diffusion in metamorphosed detrital monazites. *Earth Planet. Sci. Lett.*, **128**, 391 – 405.

Suzuki, K., Adachi, M. and Tanaka T. (1991) Middle Precambrian provenance of Jurassic sandstone in the Mino terrane, central Japan: The Th-U-total Pb evidence from an electron microprobe monazite study. *Sediment. Geol.*, **75**, 141 – 147.

Turek, A. and Kim, C. B. (1996) U-Pb zircon ages for Precambrian rocks in southwestern Ryeongnam and southwestern Gyeonggi Massifs, Korea. *Geochem. J.*, **30**, 231 – 249.

Yin, A. and Nie, S. (1993) An indentation model for the North and South China collision and the development of the Tan-Lu and Honam fault system, east Asia. *Tectonophysics*, **12**, 801 – 813.